THE JOURNAL OF BIOLOGICAL CHEMISTRY VOL. 291, NO. 34, pp. 17743–17753, August 19, 2016

Escherichia coli Topoisomerase IV E Subunit and an Inhibitor Binding Mode Revealed by NMR Spectroscopy*

Received for publication, May 10, 2016, and in revised form, June 29, 2016 Published, JBC Papers in Press, June 30, 2016, DOI 10.1074/jbc.M116.737429

Yan Li, Ying Lei Wong, Fui Mee Ng, Boping Liu, Yun Xuan Wong, Zhi Ying Poh, Shuang Liu, Siew Wen Then, Michelle Yueqi Lee, Hui Qi Ng, Qiwei Huang, Alvin W. Hung, Joseph Cherian, Jeffrey Hill, Thomas H. Keller, and CongBao Kang[1]

*From the Experimental Therapeutics Centre, Agency for Science, Technology, and Research (A*STAR), 31 Biopolis Way, Nanos, 03-01, Singapore 138669*

Bacterial topoisomerases are attractive antibacterial drug targets because of their importance in bacterial growth and low homology with other human topoisomerases. Structure-based drug design has been a proven approach of efficiently developing new antibiotics against these targets. Past studies have focused on developing lead compounds against the ATP binding pockets of both DNA gyrase and topoisomerase IV. A detailed understanding of the interactions between ligand and target in a solution state will provide valuable information for further developing drugs against topoisomerase IV targets. Here we describe a detailed characterization of a known potent inhibitor containing a 9H-pyrimido[4,5-b]indole scaffold against the N-terminal domain of the topoisomerase IV E subunit from *Escherichia coli* (eParE). Using a series of biophysical and biochemical experiments, it has been demonstrated that this inhibitor forms a tight complex with eParE. NMR studies revealed the exact protein residues responsible for inhibitor binding. Through comparative studies of two inhibitors of markedly varied potencies, it is hypothesized that gaining molecular interactions with residues in the α4 and residues close to the loop of β1-α2 and residues in the loop of β3-β4 might improve the inhibitor potency.

The emergence of antibiotic resistant bacteria is a growing and serious health problem (1). Despite the development of a limited number of new antibacterial drugs (2), there is still a shortfall of available antibiotics to effectively tackle the issue of drug-resistant bacteria (3). It is therefore important to understand the mechanisms of drug interactions on a molecular level to further our development of new antibacterial agents. Bacterial topoisomerases are well studied drug targets that are present in all bacteria and are essential for bacterial growth (4). These enzymes exhibit low structural homology with human topoisomerases and are therefore attractive drug targets. Both the DNA gyrase B subunit (GyrB)[2] and DNA topoisomerase IV E subunit (ParE) contain ATP binding pockets and are responsible for DNA replication (5, 6). Small molecule inhibition of this pocket is plausible, and a number of lead compounds have been developed targeting this pocket (7).

The availability of x-ray crystal structures of both ParE and GyrB have enabled structure-guided drug discovery (8). Past work done in the group has focused on using fragment-based approaches to develop inhibitors against GyrB (9). Further fragment-based approaches have also developed pyridylurea chemical leads against GyrB/ParE from both Gram-positive and Gram-negative bacteria (10). Gratifyingly, it has been shown that another class of inhibitors with a 9H-pyrimido[4,5-b]indole scaffold exhibited antibacterial activities (11).

X-ray crystal structures of GyrB/ParE-inhibitor complexes provide valuable information for understanding their interactions and, in turn, aid rational drug design (12–14). The ATP binding site is located at the N-terminal domain of GyrB/ParE, which makes it feasible to use a construct with a molecular weight of ~24 kDa to study target and drug interactions using different biophysical methods *in vitro*. Additionally, structural and biochemical studies revealed certain residues in the loop between β2 and α3 to be critical for the binding of novobiocin. Single mutations of residues in GyrB and ParE affected novobiocin potency by ~20-fold (15). Also, extensive work has been done in characterizing GyrB/ParE interaction with a bis-pyridylurea inhibitor (Fig. 1, *inhibitor **1***) using protein NMR spectroscopy (16–18). It has been found that this compound binds to solution forms of GyrBs/ParEs in similar modes. However, the slight difference in the amino acid sequence of the two enzymes led to markedly different inhibition potencies (18).

In an effort to understand the binding of a new class of compounds against GyrB and ParE, a potent 9H-pyrimido[4,5-b]indole was chosen to be studied (11). This new class of inhibitors was shown to have broad-spectrum antibacterial activities against both Gram-positive and Gram-negative bacteria by targeting GyrB/ParE. Residues from the loop between β2 and α3 are found to be critical for inhibitor binding and act as a cover region to the binding pocket, which may affect the rational design of potent inhibitors (18). The x-ray structures of the GyrB/ParEs and the inhibitor with a 9H-pyrimido[4,5-b]indole scaffold demonstrated that the inhibitor has a molecular interaction with residues away from the cover region, which suggested that it may bind to the target with a different mode (11).

* This work was supported by A*STAR JCO Grants 1331A028 and 1231B015. The authors declare that they have no conflicts of interest with the contents of this article.

[1] To whom correspondence should be addressed: 31 Biopolis Way, Nanos, 03-01, Singapore 138669. E-mail: cbkang@etc.a-star.edu.sg.

[2] The abbreviations used are: GyrB, DNA gyrase B subunit; ParE, DNA topoisomerase IV E subunit; eParE, DNA topoisomerase IV E subunit from *Escherichia coli*; SPR, surface plasmon resonance; HSQC, heteronuclear single quantum coherence; CSP, chemical shift perturbation; HADDOCK, high ambiguity-driven protein-protein docking; hetNOE, heteronuclear NOE; TROSY, transverse relaxation-optimized spectroscopy.

Such a binding mode may contribute to its antibacterial activity against the growth of both Gram-positive and Gram-negative bacteria. It may be a novel class of potent antibacterial agents. A further binding study in solution would allow for comparison of x-ray crystal structures with the solution structure of the ligand-protein complex. Similar to previous work on bis-pyridylurea (16–18), the binding characterization of inhibitor **2** (Fig. 1) will provide useful information for further optimization and development of this series of compounds (19–21). As compounds **1** and **2** have different structures and antibacterial activities, comparison of the binding modes of **1** and **2** with ParE will also provide insight into the antibacterial activity of **2**, which will be helpful for developing potent ParE/GyrB inhibitors.

In this study, we used NMR and other biophysical methods to understand the interactions between the N-terminal domain of *Escherichia coli* ParE (eParE) and inhibitor **2** with a 9H-pyrimido[4,5-b]indole scaffold. First, we showed that this compound has an IC_{50} of 9 nM against ParE from *E. coli*. Next, surface plasmon resonance (SPR) experiments corroborated the tight binding of **2** against eParE with a K_D of 1.1 nM. Third, we identified residues that are critical for the binding of **2** based on chemical shift perturbation (CSP) in the presence of the inhibitor. Furthermore, a hydrogen-deuterium (H-D) exchange experiment revealed residues affected by the binding of **2**. Last, we found that **2** can compete with **1** using ^{19}F NMR.

Results

Inhibitor 2 Binds to eParE and Inhibits Its Activity—GyrBs/ParEs are validated drug targets for developing antibiotics. A pyrimido-indole scaffold series developed by Truis Therapeutics was shown to have a broad-spectrum activity against both Gram-positive and Gram-negative bacteria (11). Inhibitor **2** (Fig. 1) was shown to be active against ParE of *E. coli*, with an IC_{50} of 9 nM (Fig. 2*A*). Further SPR study demonstrated that the dissociation constant (K_D) between eParE and **2** was 1.14 nM (Fig. 2*B*), which is more potent than inhibitor **1**, whose K_D was 902 nM against eParE (17).

Inhibitor 2 Can Stabilize eParE—In addition to SPR, thermal shift assays were also used to characterize ligand binding against eParE (9). As shown in Fig. 2*C*, in the absence of ligand, eParE exhibited a T_m of ~48 °C. With an excess amount of compound **2**, eParE was found to be stabilized by more than 14 °C, suggesting tight binding of the ligand to the protein. Two melting transition states could be observed with varying ligand-to-protein ratios (Fig. 2*C*). The curve corresponding to free eParE disappeared when the concentration of **2** was increased, which arose from the fact that the tight binding of the inhibitor separates the protein sample to both free and ligand-bound forms, which exhibited different melting temperatures.

NMR Study of eParE-2 Interactions—$^{1}H,^{15}N$ heteronuclear single quantum coherence (HSQC) spectra of eParE in the absence and presence of **2** were collected and compared (Fig. 3*A*). Clear chemical shift perturbations were observed, suggesting their interaction in solution. NMR titration experiments were conducted to qualitatively assess binding of **2** against eParE. As shown in Fig. 2*B*, two forms of peaks were observed in the presence of **2**. The increase in peak intensity of residues in bound form and decrease in peak intensity of residues in free form were observed when **2** was titrated into a uniformly ^{15}N-labeled eParE (Fig. 3*B*). This clearly demonstrated slow exchange interactions in solution, supporting evidence of tight binding, similar to results obtained from SPR and thermal shift experiments.

Solution Structure of the eParE-2 Complex—The backbone resonance assignments of the eParE- **2** complex were obtained by referring to the assignment of free eParE and analyzing three-dimensional NMR experiments (Fig. 4A). Most resonances in the $^{1}H,^{15}N$ HSQC spectrum were assigned (Fig. 4*A*). The secondary structure of the complex was obtained based on the assigned backbone chemical shifts using TALOS+. Eight strands and five helices were identified in the eParE-**2** complex, which is very similar to the eParE-**1** complex (17). The overall secondary structural elements are similar to those obtained from the x-ray crystal structure (PDB code 1S14), except for the N-terminal 30 residues. The difference can be attributed to the flexibility of the region. More importantly, there was no obvi-

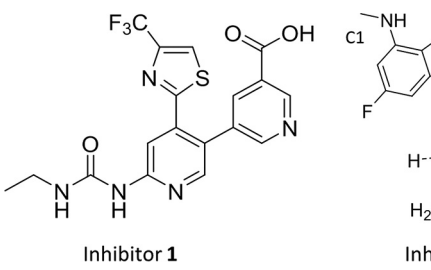

FIGURE 1. **Structures of the two inhibitors used in this study.** The structure of compound **1** is shown for comparison. The methyl group of **2** is shown as C1, and it was observed to have NOEs with residues from eParE.

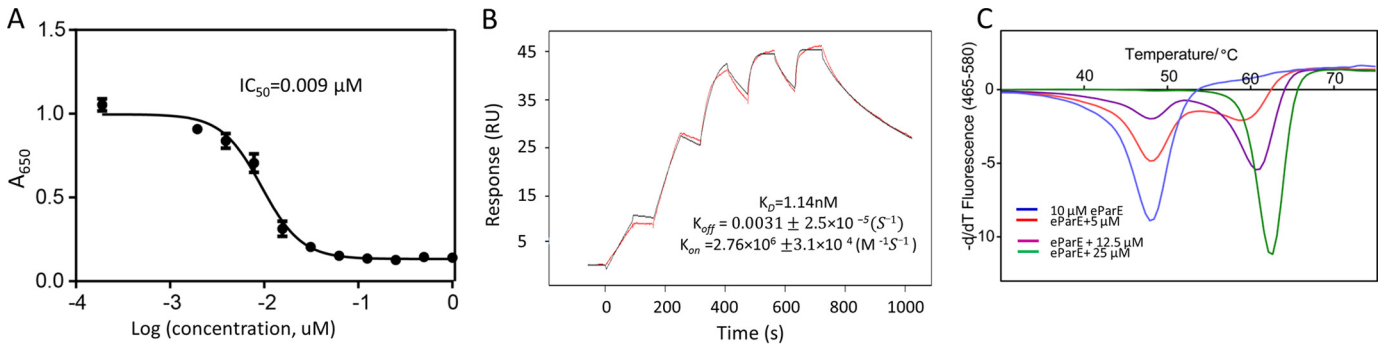

FIGURE 2. *A*, IC_{50} of **2** against ParE of *E. coli*. *B*, SPR analysis of eParE-**2** interactions. The experiment was conducted as described, and the K_D, K_{on}, and K_{off} are the association and dissociation rate constants for the complex formation and dissociation and are shown based on titration analysis. *C*, thermal shift assay of the eParE-**2** interaction. Varying concentrations of **2** were mixed with 10 μM of eParE. The curves of different samples are shown. T_m was determined based on the curve.

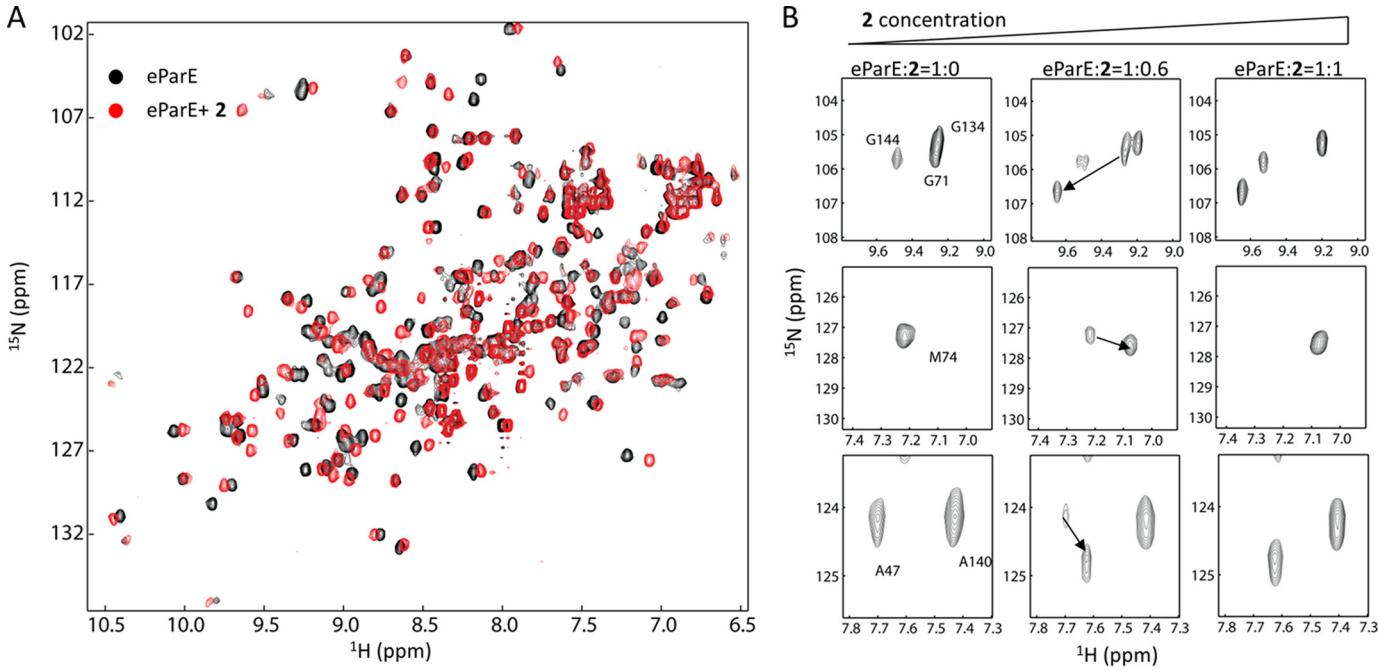

FIGURE 3. **NMR study of eParE-2 interactions.** *A*, superimposed $^{1}H,^{15}N$ HSQC spectra of eParE in the absence (*black*) and presence (*red*) of **2**. Uniformly $^{13}C/^{15}N$-labeled eParE was prepared in 0.5 mM. **2** (0.5 mM) was mixed with eParE. All experiments were conducted at 25 °C. *B*, titration of **2** into eParE. Different amounts of **2** were added into ^{15}N-labeled eParE. $^{1}H,^{15}N$ HSQC spectra were collected and superimposed. The disappearance of peaks from free eParE and appearance of peaks from the eParE-**2** complex suggests that the binding is undergoing slow exchange.

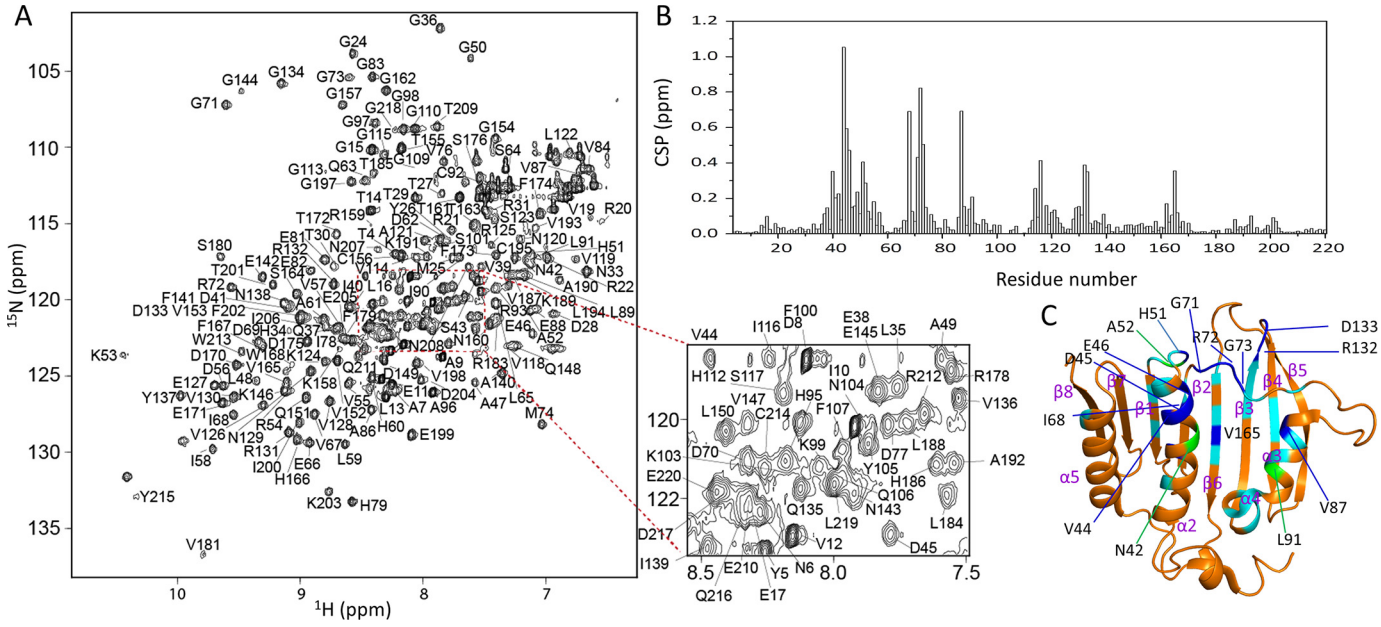

FIGURE 4. **CSP of eParE induced by inhibitor 2 binding.** *A*, assignment of the $^{1}H,^{15}N$ HSQC spectrum of the eParE-**2** complex. Assigned cross-peaks are labeled with single-letter residue name and residue number. The *highlighted region* is shown enlarged in the *right panel*. *B*, CSP of amide and amide protons caused by **2** binding. The combined chemical shift changes $(\Delta\delta) = ((\Delta\delta_{HN})^2+(\Delta\delta_N/5)^2)^{0.5}$ was plotted against residue number. *C*, residues showing CSP are mapped onto the crystal structure of eParE (PDB code 1S14). For clarity, the loop between α3 and α4 is not shown. Residues exhibiting $\Delta\delta$ of more than 0.3 ppm, between 0.3 and 0.2, and between 0.1 and 0.2 are shown in *blue*, *green*, and *cyan*, respectively.

ous secondary structural change recorded in the protein when compound **2** was added. The only noticeable difference was a slightly shorter β1 when **2** was bound to eParE (Fig. 5). Overall, the results were similar to past studies of the eParE- **1** complex, where overall secondary structures of eParE remain intact. Taken together, the results suggest that the ATP binding pocket of eParE are rigid and independent of the binding potencies of ligand toward it.

Residues of eParE Affected by Inhibitor Binding—CSP analysis is a useful tool to map an inhibitor binding interface on a target because NMR is a powerful tool to measure changes in the chemical environment of a residue. CSP of the amide protons and amide caused by **2** binding was plotted against residue number (Fig. 4*B*). The affected residues are mapped on the crystal structure of eParE (Fig. 4*C*). There are mainly eight regions affected by **2** binding. Those regions include α2, α3, α4, β2, β3,

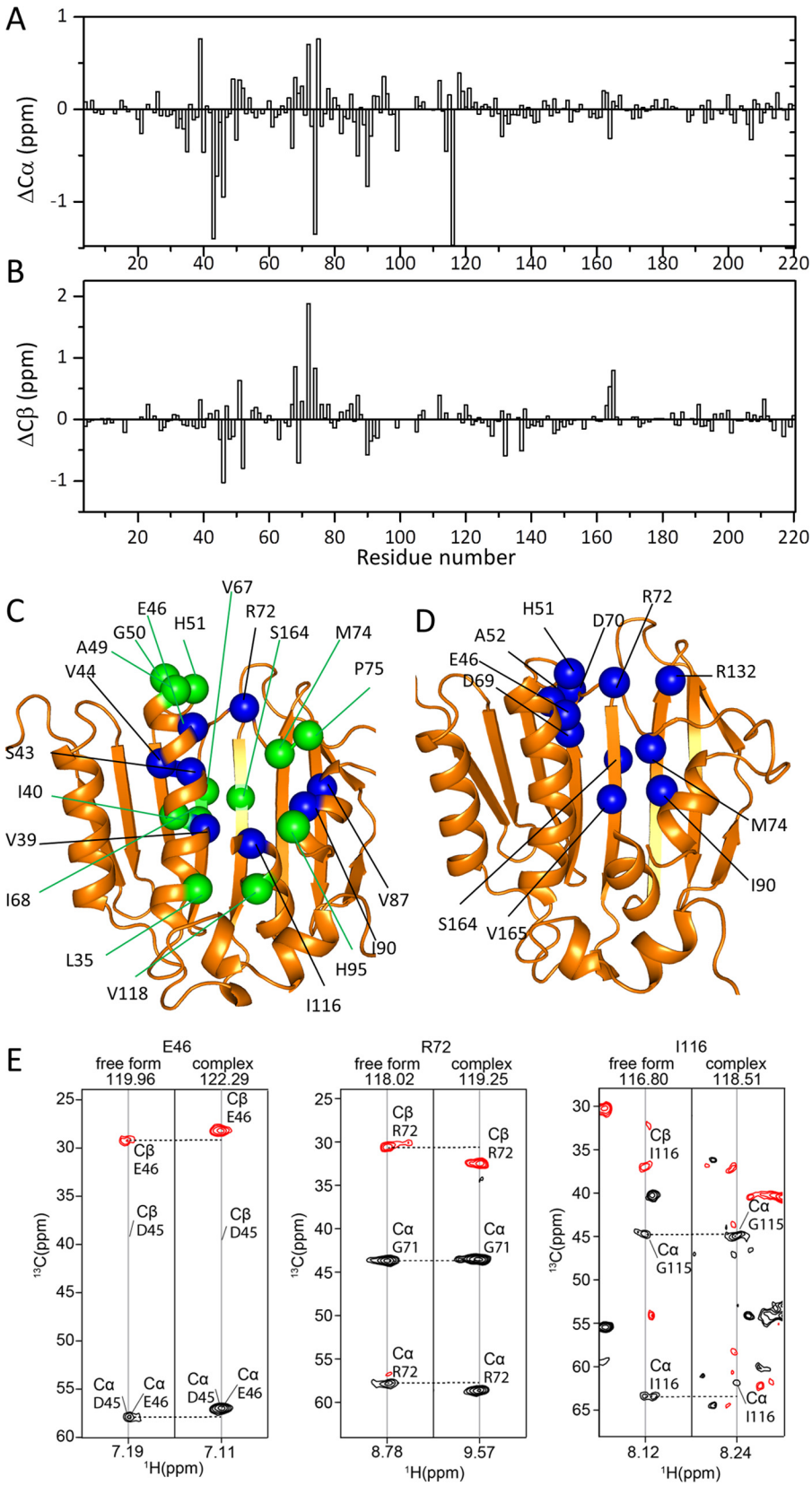

FIGURE 5. **Cα and Cβ chemical shift changes of eParE caused by inhibitor 2.** *A* and *B*, ΔCα (*A*) and ΔCβ (*B*) caused by inhibitor binding. ΔCα ($Cα_{complex}$-$Cα_{free}$) or ΔCβ ($Cβ_{complex}$-$Cβ_{free}$) is plotted against residue number. The chemical shift of free eParE was obtained from the BioMagResBank with access number 26644. *C* and *D*, residues exhibiting changes of Cα and Cβ chemical shifts were mapped onto the eParE structure. Residues with ΔCα of more than 0.5 and 0.3 ppm are shown in *blue* and *green*, respectively. Residues with ΔCβ of more than 0.5 ppm are shown in *blue*. All figures were made using PyMOL. *E*, changes of Cα and Cβ chemical shift in the presence of **2**. Strip plots of the HNCACB spectrum are shown for residues Glu-46, Arg-72, and Ile-116. Changes of Cα and Cβ chemical shifts can be observed for eParE in the absence (free form) and presence (complex) of **2**.

β6, the loop region between β2 and α3, and the loop between β1 and α2 (Fig. 4*C*). The most affected residues (Δδ > 0.3 ppm) include residues Asp-45 and Glu-46 from α2; His-51 between α2 and β1; Ile-68 from β2; Gly-71, Arg-72, and Gly-73 from the loop between α3 and β2; Val-87 from α3, and Arg-132 and Asp-133 from β3 (Fig. 4*C*). Interestingly, among these affected residues, His-51, Arg-132, and Asp-133 are not in the ATP binding pocket (Fig. 4*C*).

The chemical shifts of Cα are sensitive to the secondary structures (22). TALOS+ analysis suggested that **2** might not cause eParE to induce significant secondary structural changes. We still compared the Cα and Cβ chemical shifts of the eParE-**2** complex with those of free eParE (Fig. 5, *A* and *B*). Several residues exhibited changes in Cα upon **2** binding (Fig. 5*C*). Similar to the Δδ of amide and amide protons, seven regions exhibited Cα chemical shift changes (>0.3 ppm) upon inhibitor binding. The most affected residues include Val-39, Ile-40, Ser-43, and Val-44 from α2, Arg-72 from the loop between α3 and β2, Val-87 and Ile-90 from α3, and Ile-116 from α4 (Fig. 5). For Cβ atoms, residues including Glu-46, His-51, Ala-52, Asp-69, Asp-70, Arg-72, Met-74, Ile-90, Arg-132, Ser-164, and Val-165 exhibited obvious changes upon **2** binding (Fig. 5*D*).

*Inhibitor **2** Binds to the ATP Binding Pocket*—The crystal structure of the *E. coli* GyrB in complex with an inhibitor (C3) with a 9H-pyrimido[4,5-b]indole scaffold has been solved (11), in which the inhibitor bind to the ATP binding pocket (Fig. 6*A*). The ATP binding domain of *E. coli* ParE has a similar structure as GyrB (Fig. 6*B*). We then conducted HADDOCK using ambiguous interaction restraints derived from the CSP results. We could obtain a model showing inhibitor **2** binding to the ATP pocket (Fig. 6*B*). Residues that exhibited Cα chemical shift changes were close to the inhibitor (Fig. 6*C*). To further confirm their binding mode in solution, we collected NOESY experiments for both free eParE and its complex (Fig. 6*D*). Two unambiguous NOEs between methyl protons of C1 of **2** and amide protons of Asp-69 and Val-165 were observed (Fig. 6*D*). It was not surprising to observe only two NOEs because most of the backbone amide protons are not proximal to **2** (within 5 Å). A water signal was observed for these two residues in all the NOESY experiments, suggesting that these backbone amide protons are exposed to the solvent, which is also consistent with the structure. Nevertheless, the NOE experiments confirm the orientation of the inhibitor in the eParE ATP binding pocket, which is similar to the x-ray structure of the GyrB-C3 complex (11).

Relaxation Analysis and H-D Exchange Experiment for eParE and Its Complex—To understand the dynamic characteristics of eParE in complex with **2**, ^{15}N T_1, T_2, and NOE values were obtained (Fig. 7*A*). Consistent with the x-ray structure, most residues of eParE were stable in solution, which is characterized by high T_1 and NOE and low T_2 values (Fig. 7*A*). The C-terminal residues and N-terminal 20 residues are flexible, as evidenced by the low T_1 and NOE and high T_2 values. The loop (residues 93–115) between α3 and α4 is highly dynamic in solution. This loop exhibited no obvious change in the absence and presence of **2**, which is consistent with the fact that it is not involved in the binding. Some residues from regions of residues 40–50, 120–140, and 180–210 exhibited slightly higher het-NOEs in complex with **2**, suggesting that compound **2** can stabilize eParE. It has been noted that free eParE is stable in solution, which is similar to its complex with **2** (Fig. 7*A*).

The H-D exchange experiment was conducted to further understand the effect of **2** on the structure and dynamics of eParE. In the absence of **2**, quite a few residues from eParE were protected from exchanges, which is common for eParE with β-barrel structures (Fig. 7*B*). These residues were forming hydrogen bonds with others. A difference was observed for eParE in the absence and presence of **2**. Residues in the ATP binding pocket, including Leu-35, Gln-37, Val-39, Asn-42, Val-44, Asp-45, Ala-52, Gly-71, Gly-73, Met-74, and Ser-164, were protected from exchanges, suggesting that these residues are critical for **2** binding (Fig. 7*C*). Inhibitor **2** may prevent deuterium from entering the ATP binding pocket by forming a tight complex with eParE. Several residues away from the ATP binding pocket were also protected from exchanges in the complex (Fig. 7*B*). These residues include Ile-58, Asn-120, Ser-123, Asn-143, Lys-146, Gly-162, Phe-174, and Arg-178. These residues may form backbone hydrogen bonds with nearby residues by changing their conformations slightly when eParE binds to **2**. On the other hand, amide protons of residues including Leu-59, Gln-63, Leu-122, Ala-190, Ala-192, Lys-203, Ile-206, and Thr-209 were protected in free eParE and exposed to solvent in the complex, suggesting that these residues may lose hydrogen bond formation with nearby residues in the complex.

^{19}F NMR of Protein-Inhibitor Interactions—As **2** contains one F atom, it will give only one resonance peak in the ^{19}F spectrum. The free **2** exhibited a resonance at −75 ppm (Fig. 8*A*), which is about 12 ppm difference from **1** that was used in a previous study (Fig. 8*B*) (17). Such a difference in chemical shift arises from the different chemical groups attached to the F atoms in the compounds (Fig. 1) because the chemical shifts of F atoms are sensitive to the chemical environment (23). In the presence of eParE, chemical shift changes were observed for **2** (Fig. 8). The presence of only one ^{19}F NMR resonance observed for the complex strongly suggest a single binding mode of **2** against eParE (20). Next, ^{19}F NMR experiments were conducted to demonstrate competition of the more potent inhibitor **2** against compound **1**. A mixture containing eParE-**1** was first prepared, and ^{19}F NMR was collected (Fig. 8*B*). One resonance peak of **1** was observed for the complex. In the presence of **2**, two resonance peaks of **1** were observed (Fig. 8*B*), corresponding to the free and the eParE-bound **1**, respectively (17). The signal of **2** was also observed at ~−75.3 ppm (Fig. 8*C*). This set of established ^{19}F NMR experiments can be applied to further studies of ranking the potencies of different inhibitors against ParE using **1** as a reference compound.

Discussion

Structure-based drug design is a powerful technique that has been used in the development of potent antibacterial inhibitors (7, 24, 25). Both GyrB and ParE are validated drug targets and have attracted much drug discovery efforts around them (26, 27). However, despite the advent of many potent inhibitors against the targets, no inhibitors against GyrB and ParE have been marketed (11). The availability of high-resolution x-ray structures of GyrB/ParE-inhibitor complexes has undoubtedly

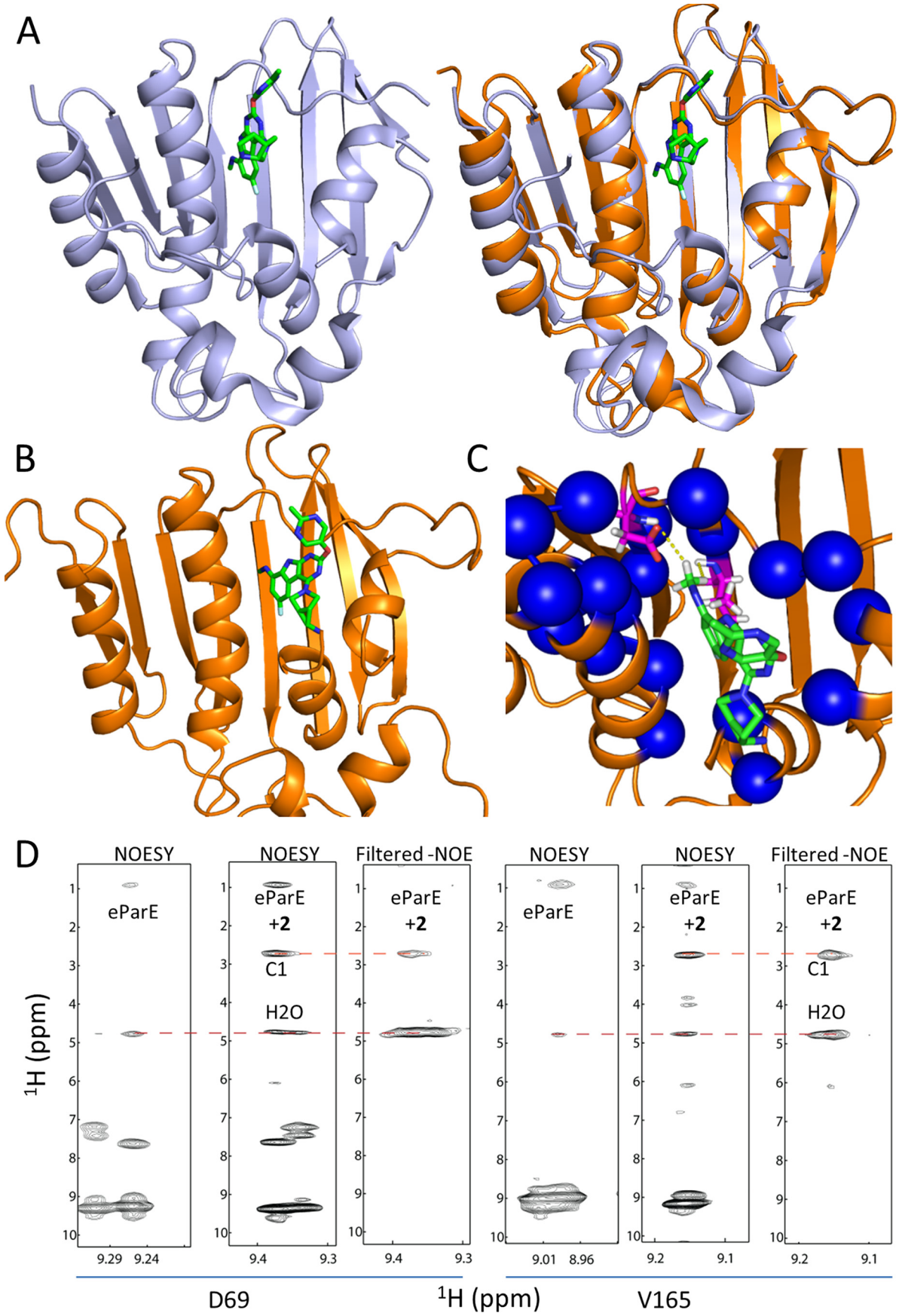
A
B
C
D
NOESY
NOESY
Filtered -NOE
NOESY
NOESY
Filtered -NOE
eParE
eParE
+2
C1
H2O
eParE
eParE
+2
C1
H2O
1H (ppm)
9.29 9.24
9.4 9.3
9.4 9.3
9.01 8.96
9.2 9.1
9.2 9.1
D69
1H (ppm)
V165

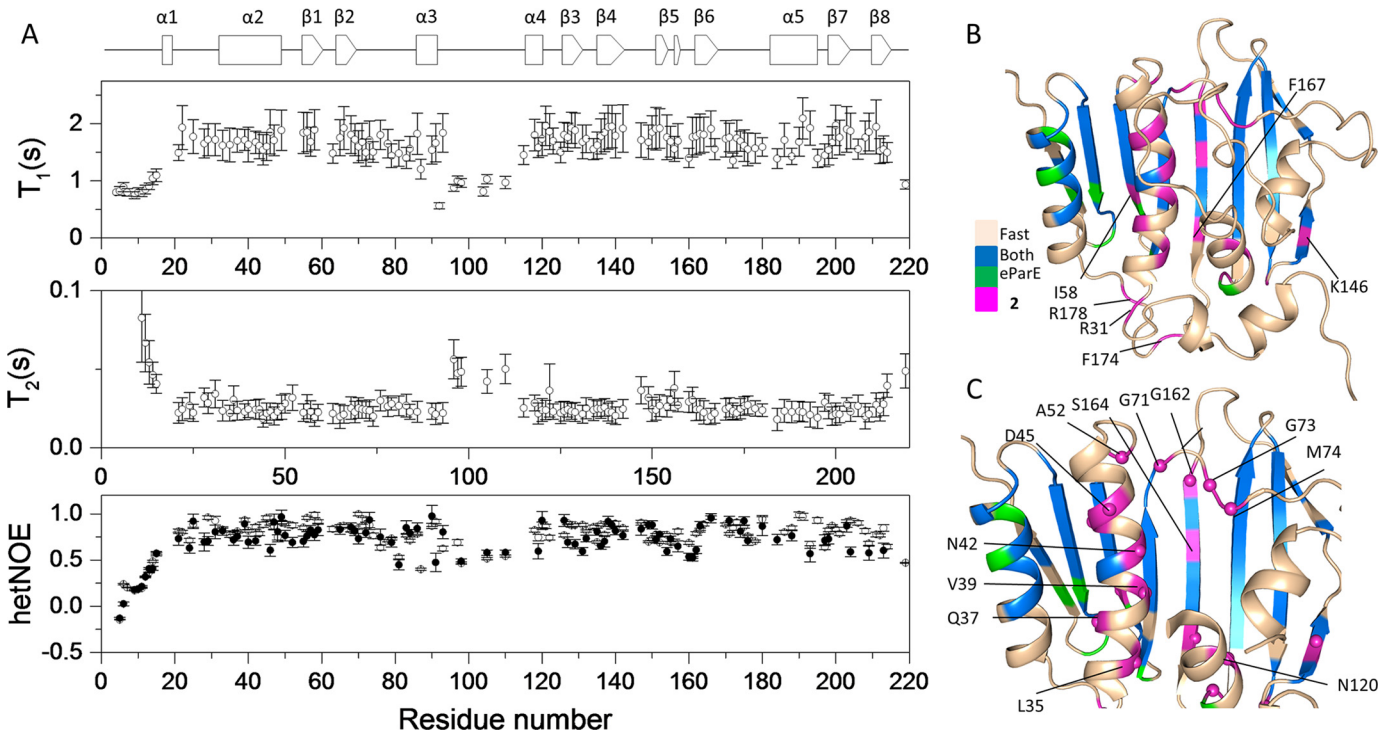

FIGURE 7. **Relaxation and H-D exchange experiment.** *A*, T_1, T_2, and hetNOE of the eParE-**2** complex. T_1 and T_2 of the eParE-**2** complex are shown in the *top* and *center panel*, respectively. The hetNOE of eParE (*black circles*) and its complex with **2** (*open circles*) are shown. *B*, residues protected from H-D exchange. Residues exposed to the solvent with 10 min (*Fast*) are shown in *wheat*. Residues protected in both eParE and the eParE-**2** complex (*Both*), free eParE only (*eParE*), and eParE-**2** complex only (**2**) are highlighted in *blue*, *green*, and *purple*, respectively. Residues that are away from the binding site are labeled with residue name and sequence number. *C*, residues in the binding pocket. Residues that were protected from exchanges when eParE formed a complex with 2 are *highlighted*. Residues that may be important for **2** binding are shown with residue name and sequence number.

been a boon toward the development of potent inhibitors against the target. In addition to x-ray structures, which provide structural information of a complex in its lowest energy state, NMR spectroscopy can provide information about target-inhibitor interactions in a more dynamic context. These solution-state structural studies will certainly complement the understanding of strategies to improve drug potencies.

In previous studies, we studied interactions of GyrB/ParE and **1**, which has a K_D of 902 nM against eParE (17). We demonstrated that **1** binds to GyrBs/ParEs from both Gram-positive and Gram-negative bacteria in the same mode (18). In this study, we studied the interaction between eParE and **2** with a K_D of 1.14 nM (Fig. 2) (11). We demonstrated that **2** formed a tight complex with eParE based on an enzymatic assay, SPR study, and thermal shift assay (Fig. 2). Further NMR study showed that residues in the ATP binding pocket were affected by the binding of **2**. CSP induced by inhibitor binding could be used to guide docking studies using HADDOCK to obtain a model to understand the interactions (Fig. 6). For both **1** and **2**, NOESY experiments can also be conducted to obtain distance restraints to validate and confirm the binding mode and determine complex structures (17) (Fig. 6). Our studies suggested that CSP-guided docking using HADDOCK is a useful and fast method to understand protein-drug interactions in a drug discovery process. It has been noted that the complex structure can also be solved for such a complex using NOE restraints because the orientation of the compound can be confirmed by using a F1-$^{13}C/^{15}N$-filtered F2-^{15}N-edited NOESY or ^{13}C-edited NOESY experiment in which the assignment of the $^{1}H,^{15}N(^{13}C)$ HSQC spectrum is available.

As **2** binds to eParE with a binding affinity (K_D = 1.14 nM) of ~900 times higher than that of **1** (K_D = 902 nM), the different residues of eParE affected by their binding may provide useful information to explain the difference in K_D values. The CSP result suggested that both inhibitors affected the chemical environment of residues from α2, α3, α4, β2, β6, and the loop region between β2 and α3 (Fig. 4). Amide and amine protons of residues His-51, Arg-132, and Asp-133 of eParE exhibited significant chemical shift changes upon binding to **2** but were not affected significantly by **1**. Residues in the loop between β1 and α2 and α4 of eParE exhibited obvious $^{13}C\alpha$ chemical shift changes upon binding to **2**, suggesting that gaining molecular interactions with residues close to these regions improved inhibitor potency. Based on the crystal structure of the

FIGURE 6. **The complex of eParE-2.** *A*, the crystal structure of GyrB of *E. coli* in complex with an inhibitor-C3. The GyrB (PDB code 4KFG) is shown as a *ribbon*, and the inhibitor is shown as *sticks*. *Right panel*, the superimposed structures of GyrB (*light blue*) and eParE (*brown*, PDB code 1S14). *B*, model of the eParE-**2** complex using HADDOCK. The inhibitor is shown as *sticks*, and protein is shown in *brown*. *C*, inhibitor binding site. The residues with ΔCα of more than 0.3 ppm are shown in *blue*. The two residues showing NOEs with the inhibitor are shown as *sticks* and are highlighted in *purple*. The observed NOEs between protein and the inhibitor are shown as *yellow dashed lines*. *D*, NOESY spectra of the free eParE and its complex. Strip plots of Asp-69 and Val-165, whose amide protons exhibited NOEs with C1 protons of **2**. For each residue, the *left panel* is a strip of NOESY of free eParE. The *center* and *right panels* are the strips of NOESY and filtered NOESY spectra of the eParE- **2** complex, respectively. The NOEs from water and protein inhibitor are highlighted with *dashed lines*.

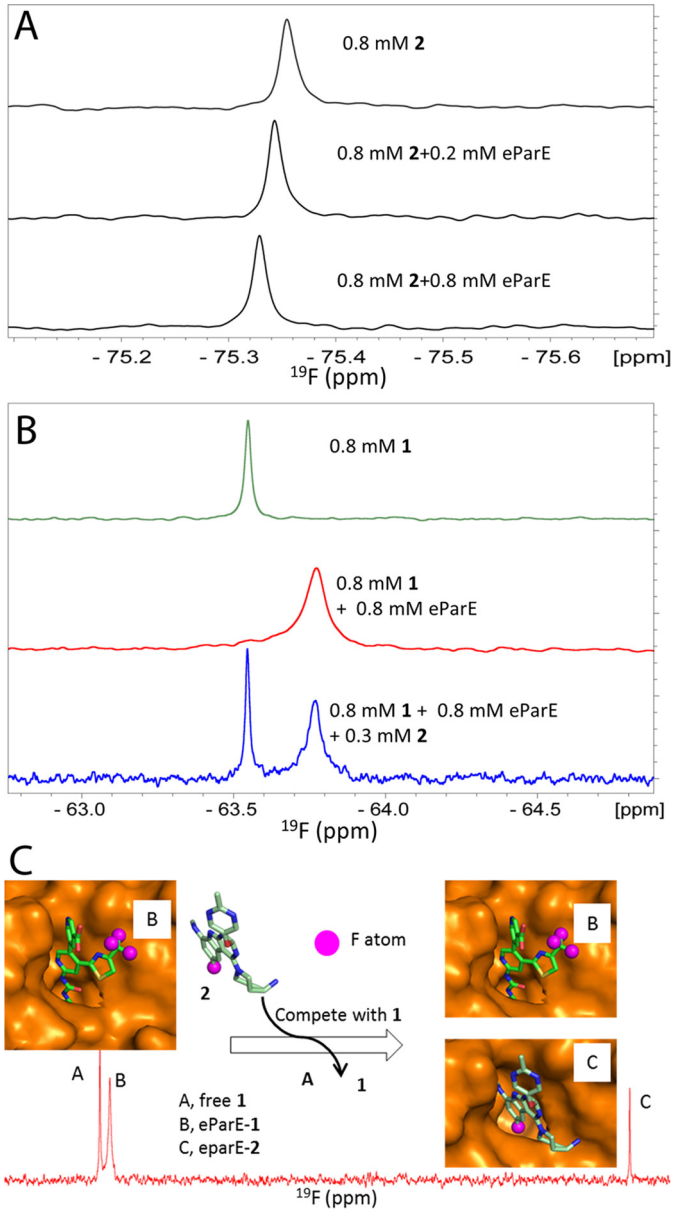

FIGURE 8. **^{19}F NMR of eParE-inhibitor interactions.** *A*, titration of eParE with **2**. ^{19}F NMR of **2** in the absence and presence of different amounts of eParE was collected and processed. *B*, competition assay using ^{19}F NMR. ^{19}F NMR spectra of free **1**, eParE-**1** complex, and eParE-**1**/**2** complex are shown in *green*, *red*, and *blue*, respectively. Appearance of the ^{19}F signal corresponding to free **1** suggests that it can be competed out of the ATP binding pocket by inhibitor **2**. *C*, model of using **1** in a competition study.

GyrB-C3 (an analog of **2**) complex, there are salt bridges between Glu-50 and Arg-76 (corresponding to residues Glu-46 and Arg-72 in eParE) that can favor a π-cation interaction with the aromatic ring of the inhibitor (Fig. 9*A*) (11). The side chains of His-55 (His-51 in eParE) form a close contact with those of Glu-50 and Arg-76. As the π-cation interaction is critical for inhibitor binding, significant CSPs were observed for residues including Glu-46 and Arg-76 of eParE. In addition, residue His-51 was affected significantly, suggesting that side chain of His-51 might be important for stabilizing the complex by forming interactions with the side chains of Glu-46 and Arg-72 (Fig. 9*B*). Residues Arg-132 and Asp-133 showed significant chemical shift changes upon inhibitor binding (Fig. 9*C*). These two residues are far away from the ATP binding pocket. The side chain of Arg-132 can form a hydrogen bond with the backbone amide of Arg-72, which might be important for stabilizing the π-cation interaction. The side chain of Arg-132 was proposed to have a hydrogen bond with the inhibitor through a water molecule (11). Arg-132 exhibited significant CSP upon inhibitor treatment (Fig. 4), suggesting that it might have a direct interaction with inhibitor **2**. NOE experiments showed that the amide proton of Met-74 exhibited stronger NOEs with water protons upon ligand binding (Fig. 9*D*), suggesting that there are water molecules close to this residue that can favor the hydrogen bond formation as proposed (11). The loop between β2 and α3 containing residues Arg-72 to Met-74 was considered as a cover region to the binding pocket. Inhibitor **2** obtained its potency by forming interactions with both this cover region and residues in β3. ParE/GyrB N-terminal binding regions are rigid in solution even in the absence of an inhibitor, which is confirmed by the relaxation experiments (Fig. 7*A*). Slight changes for residues in hetNOEs were observed for some residues of eParE in complex with **2**. A further H-D exchange experiment revealed that there might be slight conformational changes for residues distant from the binding pocket (Fig. 7). For those residues in structural proximity to the binding site of **2**, the inhibitor prevented their exposure to the solvent (Fig. 7*C*). Based on these H-D exchange experiments, residues that are critical for and affected by **2** binding were revealed, suggesting that this method will also be useful for understanding protein-drug interactions.

^{19}F NMR experiments are widely used to study ligand-protein binding and dynamics (28, 29). The simplicity and high sensitivity (natural abundance of ^{19}F = 100%) makes the application of such techniques attractive (30). Previous work has seen the application of ^{19}F NMR of **1** against eParE (17). Similar to **1**, chemical shift changes were also observed for **2** when eParE was present, suggesting its binding in solution (Fig. 8). Additionally, a ^{19}F NMR competition experiment between **1** and **2** allows for ranking of binding potencies between the two compounds and provides a rational prediction of the binding location of inhibitors. In this study, **1** was demonstrated to have both the free and the protein-bound forms when **2** was added into the premixture, indicating competitive binding (Fig. 8*B*). Furthermore, it was found through this competition experiment that **2** is more potent than **1**, corroborating binding results obtained from SPR. As ^{19}F NMR is as sensitive as ^{1}H NMR and there is no requirement for isotope labeling (30, 31), this method has been proven to be a useful tool for confirming or identifying competitive inhibitors in a drug discovery process. Our results suggested that **1** can serve as a future reference compound for confirming whether a potent GyrB/ParE inhibitor is bound to the ATP site.

In summary, biochemical and biophysical studies were performed to characterize and understand the interactions between eParE and **2**. In particular, detailed protein-based NMR studies have confirmed the solution binding mode of **2** against eParE. More importantly, through structural comparison of inhibitors **1** (K_D = 902 nM) and **2** (K_D = 1.1 nM), it is hypothesized that residues in α4, residues close to His-51 and Ala-52, such as Glu-46, Arg-72, and Arg-132, are critical for

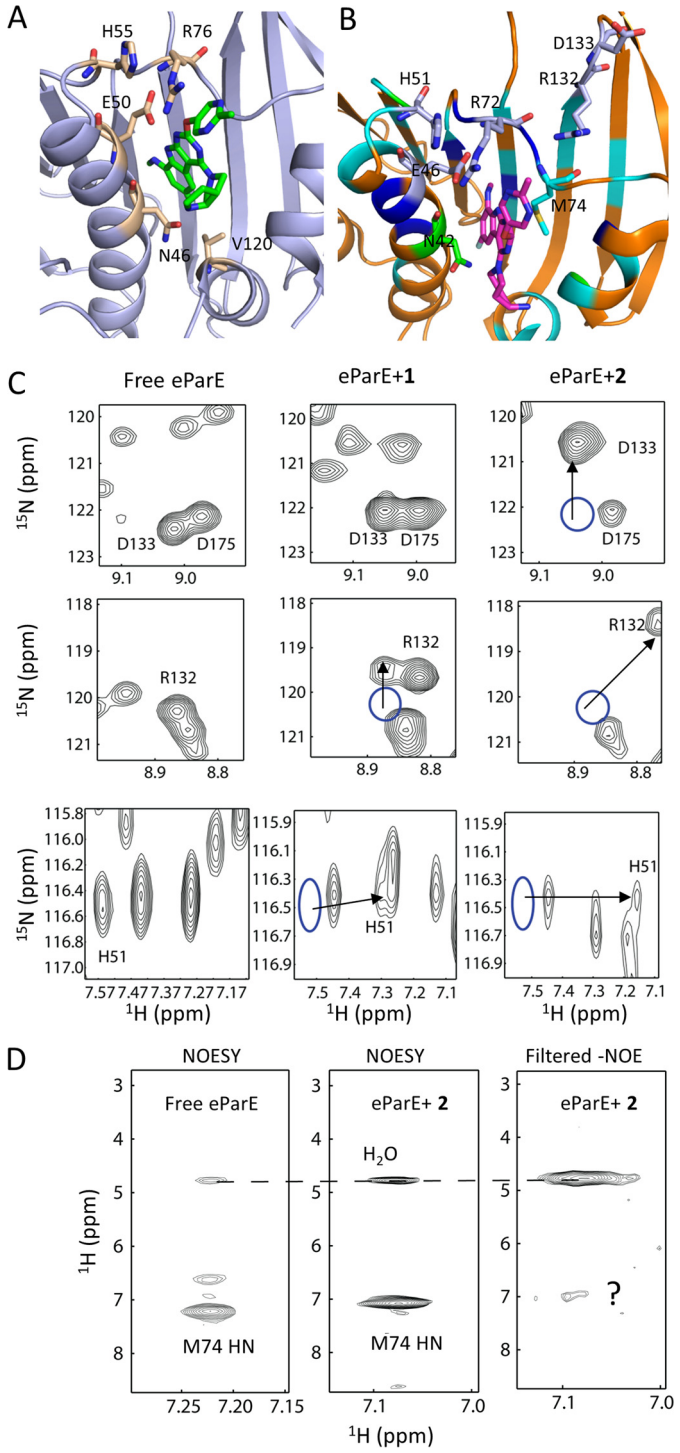

FIGURE 9. **GyrB/ParE-inhibitor interactions.** *A*, structure of the GyrB-C3 complex. The C3 inhibitor is shown as *sticks* (PDB code 4KFG). Several residues that might be important for improving inhibitor potency are shown as *sticks*. *B*, structural model of the eParE-**2** complex. The model was from HADDOCK based on CSP caused by **2** binding. Inhibitor **2** is shown as *sticks*. Glu-46 and Arg-72 might form salt bridges to favor interaction with **2**. Residues exhibiting CSP upon inhibitor binding are shown in *blue*, *green*, and *cyan*, respectively. Arg-132 and Asp-133, which showed significant CSPs, are shown in *light blue*. Met-74 is shown as *sticks*, and its amide proton exhibited NOEs with water protons. *C*, ^{1}H,^{15}N HSQC spectra of eParE in the absence and presence of **1** and **2**. These three residues exhibited difference when eParE bound to **1** and **2**. The peak corresponding to free eParE is shown as a *circle*. *Arrows* indicate the direction of peak shifting after inhibitor binding. The assignment of the eParE-**1** complex was obtained from a previous report. *D*, strip plot of Met-74 in the NOESY spectra. The amide proton of Met-74 exhibited NOEs with water protons. For each residue, the *left panel* is a strip of NOESY of free eParE. The *center* and *right panels* are the strips of NOESY and filtered NOESY spectra of the eParE-**2** complex, respectively. The peak labeled with a *question mark* might be a NOE with the inhibitor, which cannot be unambiguously assigned.

inhibitor potency against eParE. This in-depth understanding of ligand-ParE interactions at a molecular level will potentially guide and impact future development of topoisomerase inhibitors.

Experimental Procedures

Protein Production and Inhibitor Synthesis—The N-terminal ATP binding domain comprising residues 1–218 of eParE was expressed and purified as described previously (16). Briefly, the pET29b vector harboring the cDNA of eParE and a C-terminal tag (LEHHHHHH) was transformed into *E. coli* BL21(DE3)-competent cells. Recombinant protein was induced at 18 °C by adding 1 mM isopropyl 1-thio-β-D-galactopyranoside overnight when the cell optical density reached 0.8–1.0. The recombinant eParE was purified using nickel-nitrilotriacetic acid resin and gel filtration chromatography. Protein was concentrated to 0.5–0.8 mM in an NMR buffer that contained 20 mM sodium phosphate (pH 6.5), 150 mM KCl, 2 mM DTT, and 0.5 mM EDTA. Uniformly ^{13}C/^{15}N, ~70% ^{2}H-labeled eParE was prepared for NOESY data collection. Compounds **1** and **2** (Fig. 1) were synthesized as described in the literature (11). A stock solution was prepared by dissolving the powder into deuterated DMSO.

Thermal Shift Assay—The thermal shift experiment was carried out using SYPRO Orange dye on a Roche LC480 PCR machine using a similar method as described previously (18, 32). A 384-well plate was used in the assay, in which each well contained 10 μM eParE with 20 × SYPRO Orange. The assay buffer contained 20 mM sodium phosphate, 150 mM KCl, 2 mM DTT, and 0.5 mM EDTA (pH 7.2). Varying concentrations of **2** from 0–25 μM were mixed with eParE. The samples were subjected to temperature increases from 30–95 °C. GraphPad Prism (GraphPad) was used to generate the melting curve.

IC_{50} Assay for eParE—The effect of **2** on ATP hydrolysis was measured, and the IC_{50} is defined as the inhibitor concentration that gives 50% of maximum enzymatic activity. All reactions were performed in 30-μl volumes in a transparent 384-well plate (17). Mixtures that contained **2** with concentrations varying from 0.39–200 μM were prepared. The assay mixtures also contained 20 mM Tris-HCl (pH 8.0), 8 mM $MgCl_2$, 50 mM ammonium acetate, 2.5% (v/v) glycerol, 0.005% (v/v) Brij 35, 0.5 mM EDTA, 5 mM DTT, 2% DMSO, 2 μM ParC, 2 μM full-length ParE, 160 μM ATP, and 0.005 mg/ml salmon sperm DNA (17). The mixtures were first incubated at room temperature for 24 h, and the reaction was quenched by addition of 30 μl of a reagent that contained 0.34 mg/ml of malachite green chloride and 0.011 g/ml ammonium molybdate that was prepared in 1 M HCl. The absorbance at 650 nm (A_{650}) was measured after incubation at room temperature for 5 min. The A_{650} was plotted against compound concentration (log), and the IC_{50} value was obtained.

Surface Plasmon Resonance Measurement—The SPR experiment was carried out to obtain the binding affinity between

eParE and **2** on a BIAcore-2000 system (GE Healthcare). CM5 chips were used to analyze protein-**2** interactions. The experiment was carried out at 25 °C. Purified eParE was first immobilized on a chip. A buffer that contained 10 mM HEPES (pH 7.5), 150 mM NaCl, 3 mM EDTA, and 0.005% v/v surfactant P20 was filtered and degassed. **2** in DMSO was diluted with the buffer before injection. The data were analyzed using software provided with the equipment. The K_D value was obtained using a 1:1 steady-state binding model (18).

Ligand-observed ^{19}F Experiments—As **2** contains only one F atom, ^{19}F NMR experiments were carried out at room temperature on a Bruker 400 MHz magnet that was equipped with a broadband observe probe. Free inhibitor was prepared in the NMR buffer. For eParE-inhibitor mixtures, different amounts of eParE samples were first lyophilized. The lyophilized sample was then mixed with **2** that was in water instead of buffer because the lyophilized sample contained salts. The spectra were collected and processed using Topspin 2.1. For competition with **1**, a protein mixture containing 0.8 mM inhibitor **1** and 0.8 mM eParE was first prepared. A ^{19}F spectrum was acquired and processed. Different amounts of **2** were then added, followed by ^{19}F spectrum acquisition and processing. Observation of a peak corresponding to free **1** implies that it can be competed out of the binding pocket by **2**.

NMR Experiments—All NMR experiments were collected at 25 °C on a Bruker 700- or 600-MHz magnet equipped with a cryoprobe. The backbone assignment of eParE in complex with **2** was obtained based on two- and three-dimensional experiments. Transverse relaxation-optimized spectroscopy (TROSY) (33, 34)-based experiments, including two-dimensional TROSY, three-dimensional HNCACB, HNCOCACB, and HNCO were collected. The collected spectra were processed using NMRPipe (35) and Topspin 2.1. The spectra were analyzed using NMRView (36) and CARA, which was developed in the Wüthrich group. Backbone assignment was conducted based on the three-dimensional experiments and the previous assignment of free eParE (37). The secondary structure was analyzed using TALOS+ based on the obtained backbone chemical shifts (38).

To map the inhibitor binding site on eParE, ^{1}H,^{15}N TROSY, or HSQC spectra of eParE in the absence and presence of **2** were collected and superimposed. CSP caused by **2** binding were mapped onto the crystal structure of eParE (39). The combined chemical shift changes ($\Delta\delta$) were determined using the following equation: $\Delta\delta = ((\Delta\delta_{HN})^2 + (\Delta\delta_N/5)^2)^{0.5}$, where $\Delta\delta_{HN}$ and $\Delta\delta_N$ are the CSPs caused by **2** binding in the amide proton and amide dimensions, respectively (39). The Cα and Cβ chemical shifts of the complex were also compared with those in free form. To further confirm the model obtained by a docking method, NOEs between protein and the inhibitor was obtained by comparing the NOESY spectra of free eParE and the eParE-inhibitor complex and an F1-^{13}C/^{15}N-filtered F2-^{15}N-edited NOESY experiment of the complex. A mixing time of 120 ms was used in all NOESY experiments.

^{15}N-T_1, T_2 and heteronuclear NOEs (hetNOE) were measured using triple-labeled eParE in the absence and presence of **2**. Because of the signal overlap, only hetNOEs were compared for eParE and its complex. T_1 values were obtained from a pseudo-three-dimensional experiment with relaxation delays of 200, 400, 600, 800, 1000, 1200, 1600, and 2000 ms. T_2 values were obtained from a series of two-dimensional ^{1}H,^{15} HSQC spectra from a pseudo-three-dimensional experiment with relaxation delays of 17, 34, 51, 68, 85, 102, 119, 136, and 153 ms. Because of the signal intensities, only the first six data points were used for T_2 determination. The hetNOEs were obtained from spectra collected without and with 3 s presaturation.

The hydrogen-deuterium exchange experiment was conducted using similar methods as described previously (32). Briefly, lyophilized eParE in the absence and presence of an equimolar ratio of **2** were prepared. D_2O was added to the samples, and a series of ^{1}H,^{15}N HSQC spectra were collected and compared. All experiments were conducted at 298 K, and the spectra were collected and processed as mentioned before.

High Ambiguity-driven Protein-Protein Docking (HADDOCK)—HADDOCK was used to understand protein-inhibitor interactions. The ambiguous interaction restraints were based on residues that exhibited a $\Delta\delta$ of more than 0.3 ppm upon **2** binding. The restraints were generated using the HADDOCK server (40). The eParE structure was obtained from the PDB (PDB code 1SA4). The structure of the inhibitor was generated using the PRODRG server (41). The topology and parameter files of the inhibitor for HADDOCK were generated using HIP-UP (42). The docking was conducted on a local computer using HADDOCK2.1.

Author Contributions—C. K., T. H. K., and J. H. designed the experiments. T. H. K. and J. C. selected inhibitor **2**. Y. L. conducted the NMR experiments. Y. L. and C. K. analyzed the results. F. M. N., S. W. T., and J. H. conducted the biochemical analysis of ParE. S. L. and A. W. H. conducted the thermal shift study. B. L. and J. H. conducted SPR and analyzed the SPR result. Y. X. W., Z. Y. P., and J. C. synthesized the compounds. Y. L. W., M. Y. L., H. Q. N., and Q. H. purified protein. C. K. drafted the manuscript, and all authors revised and approved the manuscript.

*Acknowledgments—We appreciate valuable discussions with members of the drug discovery team in the Experimental Therapeutics Centre, A*STAR.*

References

1. Silver, L. L. (2011) Challenges of antibacterial discovery. *Clin. Microbiol. Rev.* **24,** 71–109
2. Miller, J. R., and Waldrop, G. L. (2010) Discovery of novel antibacterials. *Expert Opin. Drug Discov.* **5,** 145–154
3. Fischbach, M. A., and Walsh, C. T. (2009) Antibiotics for emerging pathogens. *Science* **325,** 1089–1093
4. Maxwell, A. (1997) DNA gyrase as a drug target. *Trends Microbiol.* **5,** 102–109
5. Champoux, J. J. (2001) DNA topoisomerases: structure, function, and mechanism. *Annu. Rev. Biochem.* **70,** 369–413
6. Stanger, F. V., Dehio, C., and Schirmer, T. (2014) Structure of the N-terminal Gyrase B fragment in complex with ADPPi reveals rigid-body motion induced by ATP hydrolysis. *PLoS ONE* **9,**e107289
7. Škedelj, V., Tomašić, T., Mašić, L. P., and Zega, A. (2011) ATP-binding site of bacterial enzymes as a target for antibacterial drug design. *J. Med. Chem.* **54,** 915–929
8. Campos-Olivas, R. (2011) NMR screening and hit validation in fragment based drug discovery. *Curr. Top. Med. Chem.* **11,** 43–67
9. Chen, G.-Y., Ng, F. M., Tan, Y. W., Poulsen, A., Seetoh, W., Lin, G., Kang,

C., Then, S. W., Ahmad, N. H., Wong, Y. L., Ng, H. Q., Chia, C. S. B., Lau, Q. Y., Hill, J., Hung, A. W., and Keller, T. H. (2015) Application of fragment-based drug discovery against DNA gyrase B. *ChemPlusChem* **80,** 1250–1254

10. Basarab, G. S., Manchester, J. I., Bist, S., Boriack-Sjodin, P. A., Dangel, B., Illingworth, R., Sherer, B. A., Sriram, S., Uria-Nickelsen, M., and Eakin, A. E. (2013) Fragment-to-hit-to-lead discovery of a novel pyridylurea scaffold of ATP competitive dual targeting type II topoisomerase inhibiting antibacterial agents. *J. Med. Chem.* **56,** 8712–8735
11. Tari, L. W., Li, X., Trzoss, M., Bensen, D. C., Chen, Z., Lam, T., Zhang, J., Lee, S. J., Hough, G., Phillipson, D., Akers-Rodriguez, S., Cunningham, M. L., Kwan, B. P., Nelson, K. J., Castellano, A., *et al.* (2013) Tricyclic GyrB/ParE (TriBE) inhibitors: a new class of broad-spectrum dual-targeting antibacterial agents. *PLoS ONE* **8,** e84409
12. Wigley, D. B., Davies, G. J., Dodson, E. J., Maxwell, A., and Dodson, G. (1991) Crystal structure of an N-terminal fragment of the DNA gyrase B protein. *Nature* **351,** 624–629
13. Tsai, F. T., Singh, O. M., Skarzynski, T., Wonacott, A. J., Weston, S., Tucker, A., Pauptit, R. A., Breeze, A. L., Poyser, J. P., O'Brien, R., Ladbury, J. E., and Wigley, D. B. (1997) The high-resolution crystal structure of a 24-kDa gyrase B fragment from *E. coli* complexed with one of the most potent coumarin inhibitors, clorobiocin. *Proteins* **28,** 41–52
14. Lübbers, T., Angehrn, P., Gmünder, H., Herzig, S., and Kulhanek, J. (2000) Design, synthesis, and structure-activity relationship studies of ATP analogues as DNA gyrase inhibitors. *Bioorg. Med. Chem. Lett.* **10,** 821–826
15. Bellon, S., Parsons, J. D., Wei, Y., Hayakawa, K., Swenson, L. L., Charifson, P. S., Lippke, J. A., Aldape, R., and Gross, C. H. (2004) Crystal structures of *Escherichia coli* topoisomerase IV ParE subunit (24 and 43 kilodaltons): a single residue dictates differences in novobiocin potency against topoisomerase IV and DNA gyrase. *Antimicrob. Agents Chemother.* **48,** 1856–1864
16. Li, Y., Wong, Y. X., Poh, Z. Y., Wong, Y. L., Lee, M. Y., Ng, H. Q., Liu, B., Hung, A. W., Cherian, J., Hill, J., Keller, T. H., and Kang, C. (2015) NMR structural characterization of the N-terminal active domain of the gyrase B subunit from *Pseudomonas aeruginosa* and its complex with an inhibitor. *FEBS Lett.* **589,** 2683–2869
17. Li, Y., Wong, Y. L., Ng, F. M., Liu, B., Wong, Y. X., Poh, Z. Y., Then, S. W., Lee, M. Y., Ng, H. Q., Hung, A. W., Cherian, J., Hill, J., Keller, T. H., and Kang, C. (2015) Characterization of the interaction between *Escherichia coli* topoisomerase IV E subunit and an ATP competitive inhibitor. *Biochem. Biophys. Res. Commun.* **467,** 961–966
18. Kang, C., Li, Y., Cherian, J., Liu, B., Ng, H. Q., Lee, M. Y., Binte Ahmad, N. H., Poh, Z. Y., Wong, Y. X., Huang, Q., Wong, Y. L., Hung, A. W., Hill, J., and Keller, T. H. (2015) Biophysical studies of bacterial topoisomerases substantiate their binding modes to an inhibitor. *Biophys. J.* **109,** 1969–1977
19. Vajpai, N., Strauss, A., Fendrich, G., Cowan-Jacob, S. W., Manley, P. W., Grzesiek, S., and Jahnke, W. (2008) Solution conformations and dynamics of ABL kinase-inhibitor complexes determined by NMR substantiate the different binding modes of imatinib/nilotinib and dasatinib. *J. Biol. Chem.* **283,** 18292–18302
20. Hughes, T. S., Giri, P. K., de Vera, I. M., Marciano, D. P., Kuruvilla, D. S., Shin, Y., Blayo, A.-L., Kamenecka, T. M., Burris, T. P., Griffin, P. R., and Kojetin, D. J. (2014) An alternate binding site for PPARγ ligands. *Nat. Commun.* **5,** 3571–3583
21. Dias, D. M., Furtado, J., Wasielewski, E., Cruz, R., Costello, B., Cole, L., Faria, T. Q., Baaske, P., Brito, R. M., Ciulli, A., Simões, I., Macedo-Ribeiro, S., Faro, C., Geraldes, C. F., and Castanheira, P. (2016) Biophysical characterization of laforin-carbohydrate interaction. *Biochem. J.* **473,** 335–345
22. Saitô, H., Ando, I., and Ramamoorthy, A. (2010) Chemical shift tensor: the heart of NMR: insights into biological aspects of proteins. *Prog. Nucl. Magn. Reson. Spectrosc.* **57,** 181–228
23. Vulpetti, A., Landrum, G., Rüdisser, S., Erbel, P., and Dalvit, C. (2010) 19F NMR chemical shift prediction with fluorine fingerprint descriptor. *J. Fluor. Chem.* **131,** 570–577
24. Brvar, M., Perdih, A., Renko, M., Anderluh, G., Turk, D., and Solmajer, T. (2012) Structure-based discovery of substituted 4,5′-bithiazoles as novel DNA gyrase inhibitors. *J. Med. Chem.* **55,** 6413–6426
25. Manchester, J. I., Dussault, D. D., Rose, J. A., Boriack-Sjodin, P. A., Uria-Nickelsen, M., Ioannidis, G., Bist, S., Fleming, P., and Hull, K. G. (2012) Discovery of a novel azaindole class of antibacterial agents targeting the ATPase domains of DNA gyrase and topoisomerase IV. *Bioorg. Med. Chem. Lett.* **22,** 5150–5156
26. Mitscher, L. A. (2005) Bacterial topoisomerase inhibitors: quinolone and pyridone antibacterial agents. *Chem. Rev.* **105,** 559–592
27. Grossman, T. H., Bartels, D. J., Mullin, S., Gross, C. H., Parsons, J. D., Liao, Y., Grillot, A. L., Stamos, D., Olson, E. R., Charifson, P. S., and Mani, N. (2007) Dual targeting of GyrB and ParE by a novel aminobenzimidazole class of antibacterial compounds. *Antimicrob. Agents Chemother.* **51,** 657–666
28. Suzuki, Y., Brender, J. R., Hartman, K., Ramamoorthy, A., and Marsh, E. N. (2012) Alternative pathways of human islet amyloid polypeptide aggregation distinguished by (19)f nuclear magnetic resonance-detected kinetics of monomer consumption. *Biochemistry* **51,** 8154–8162
29. Suzuki, Y., Brender, J. R., Soper, M. T., Krishnamoorthy, J., Zhou, Y., Ruotolo, B. T., Kotov, N. A., Ramamoorthy, A., and Marsh, E. N. (2013) Resolution of oligomeric species during the aggregation of Aβ1–40 using (19)F NMR. *Biochemistry* **52,** 1903–1912
30. Didenko, T., Liu, J. J., Horst, R., Stevens, R. C., and Wuthrich, K. (2013) Fluorine-19 NMR of integral membrane proteins illustrated with studies of GPCRs. *Curr. Opin. Struct. Biol.* **5,** 740–747
31. Entress, R. M., Dancer, R. J., O'Brien, D. P., Try, A. C., Cooper, M. A., and Williams, D. H. (1998) 19F NMR in the measurement of binding affinities of chloroeremomycin to model bacterial cell-wall surfaces that mimic VanA and VanB resistance. *Chem. Biol.* **5,** 329–337
32. Gayen, S., Li, Q., Chen, A. S., Nguyen, T. H., Huang, Q., Hill, J., and Kang, C. (2011) An NMR study of the N-terminal domain of wild-type hERG and a T65P trafficking deficient hERG mutant. *Proteins* **79,** 2557–2565
33. Pervushin, K., Ono, A., Fernández, C., Szyperski, T., Kainosho, M., and Wüthrich, K. (1998) NMR scalar couplings across Watson-Crick base pair hydrogen bonds in DNA observed by transverse relaxation-optimized spectroscopy. *Proc. Natl. Acad. Sci. U.S.A.* **95,** 14147–14151
34. Salzmann, M., Pervushin, K., Wider, G., Senn, H., and Wüthrich, K. (1998) TROSY in triple-resonance experiments: new perspectives for sequential NMR assignment of large proteins. *Proc. Natl. Acad. Sci. U.S.A.* **95,** 13585–13590
35. Delaglio, F., Grzesiek, S., Vuister, G. W., Zhu, G., Pfeifer, J., and Bax, A. (1995) NMRPipe: a multidimensional spectral processing system based on UNIX pipes. *J. Biomol. NMR* **6,** 277–293
36. Johnson, B. A. (2004) Using NMRView to visualize and analyze the NMR spectra of macromolecules. *Methods Mol. Biol.* **278,** 313–352
37. Li, Y., Wong, Y. L., Lee, M. Y., Ng, H. Q., and Kang, C. (2016) Backbone assignment of the N-terminal 24-kDa fragment of *Escherichia coli* topoisomerase IV ParE subunit. *Biomol. NMR Assign.* **10,** 135–138
38. Shen, Y., Delaglio, F., Cornilescu, G., and Bax, A. (2009) TALOS+: a hybrid method for predicting protein backbone torsion angles from NMR chemical shifts. *J. Biomol. NMR* **44,** 213–223
39. Williamson, M. P. (2013) Using chemical shift perturbation to characterise ligand binding. *Prog. Nucl. Magn. Reson. Spectrosc.* **73,** 1–16
40. de Vries, S. J., van Dijk, A. D., Krzeminski, M., van Dijk, M., Thureau, A., Hsu, V., Wassenaar, T., and Bonvin, A. M. (2007) HADDOCK versus HADDOCK: new features and performance of HADDOCK2.0 on the CAPRI targets. *Proteins* **69,** 726–733
41. Schüttelkopf, A. W., and van Aalten, D. M. (2004) PRODRG: a tool for high-throughput crystallography of protein-ligand complexes. *Acta Crystallogr. D Biol. Crystallogr.* **60,** 1355–1363
42. Kleywegt, G. J. (2007) Crystallographic refinement of ligand complexes. *Acta Crystallogr. D Biol. Crystallogr.* **63,** 94–100